Project Report
TIP-92

Quantum Network Testbed and Technology Development: FY18 Quantum System Sciences Technical Investment Program

P.B. Dixon
M.E. Grein
C. Lee
R.P. Murphy
G.R. Steinbrecher
H. Zhang

12 February 2019

Lincoln Laboratory
MASSACHUSETTS INSTITUTE OF TECHNOLOGY
LEXINGTON, MASSACHUSETTS

This material is based upon work supported by the United States Air Force under Air Force Contract No. FA8721-05-C-0002 and/or FA8702-15-D-0001.

This report is the result of studies performed at Lincoln Laboratory, a federally funded research and development center operated by Massachusetts Institute of Technology. This material is based on work supported under Air Force Contract No. FA8721-05-C-0002 and/or FA8702-15-D-0001. Any opinions, findings and conclusions or recommendations expressed in this material are those of the authors and do not necessarily reflect the views of the U.S. Air Force.

Massachusetts Institute of Technology
Lincoln Laboratory

Quantum Network Testbed and Technology Development: FY18 Quantum System Sciences Technical Investment Program

P.B. Dixon
M.E. Grein
C. Lee
R.P. Murphy
G.R. Steinbrecher
H. Zhang
Group 67

Project Report TIP-92

12 February 2019

Lexington Massachusetts

EXECUTIVE SUMMARY

The quantum network testbed and technology development program, part of the Quantum Systems Science line program, seeks to build the technological components required for quantum networking and to integrate them into a deployed-fiber testbed. The multi-year outline of our program is a phased development approach that allows us to demonstrate important quantum networking capabilities in the near term while still developing infrastructure to build toward far-term applications. The first and simplest phase is direct transmission: producing entangled pairs at one node and transmitting one photon to the other node, so the two nodes share entanglement. This phase was demonstrated in FY17. The next phase, multi-span networking with synchronization, was a significant part of our FY18 program.

We built two new entangled-photon-pair sources designed to produce the high-visibility quantum interference required for multi-span networking, and we built a system to swap entanglement between them. So far, we have demonstrated a quantum interference visibility of 91% and single-source entanglement visibilities of 92% and above. We also developed two different synchronization schemes, the first of which is specifically intended to synchronize the repetition rates of remote entanglement sources. Preliminary measurements of this first scheme show excess timing jitter of 60 ps, and we expect to reduce this excess jitter in improved tests. The second scheme is a more general method for sharing time and frequency that offers greater functionality; for example, this scheme could be used for synchronizing not only the repetition rates but also the phase between two clocks. Additionally, we packaged new integrated photonic devices and used an integrated photonic system as an optical switch to reduce packet loss and latency in a (classical) communication network via optical flow switching.

Our FY18 efforts have laid the groundwork for synchronizing the generation and distribution of entanglement across deployed fiber links. In particular, we have interacted photons produced by independent entanglement sources. We have also made progress toward connecting and comparing remote atomic clocks to perform single-span stabilization of the deployed fiber and eventually integrate trapped ion systems and other quantum processor and memory technologies into the quantum network testbed. Our FY19 efforts will continue to combine the synchronization and fiber stabilization with the entanglement sources to demonstrate quantum communication protocols in the testbed and explore preliminary demonstrations of quantum network applications that could provide advantages over their classical counterparts.

TABLE OF CONTENTS

LIST OF FIGURES AND TABLES

1. SPECTRALLY PURE SOURCES OF POLARIZATION ENTANGLEMENT

In FY18 we worked toward multi-span quantum networking capabilities, specifically focusing on swapping entanglement between independent polarization-entangled photon pairs. For a successful entanglement swap, we require both high spectral purity and high-quality polarization entanglement. Our targets for each property were 90% spectral purity and 90% entanglement visibility.

For entanglement swapping, we built two identical polarization-entangled photon-pair sources. Each source is based on spontaneous parametric downconversion (SPDC) in a bulk periodically poled potassium titanyl phosphate (PPKTP) crystal. The sources are engineered to produce photons in spectrally pure biphoton states --- a requirement for high-visibility quantum interference between photons produced by independent sources. Our recipe for spectral purity has two main components:

1. Engineering the phasematching functions to generate the desired crystal properties via a custom poling mask, and

2. Correlating the spectral bandwidth of the pump beam with the engineered crystal phasematching bandwidth, such that the ratio of the two bandwidths matches a theoretically predicted scaling factor.

The custom-poled crystals have a phasematching bandwidth of 1.7 nm around 1582 nm. To pump the crystals, we have acquired a Spectra-Physics Tsunami Titanium-Sapphire mode-locked laser that produces transform-limited, sech^2-shaped pulses with approximately 0.6 nm of optical bandwidth around 791 nm, at a repetition rate of 80 MHz.

One figure of merit for source quality is spectral purity, and a quick method of estimating the spectral purity is to measure the joint spectral intensity (JSI) between the downconverted signal and idler photons. The sources are engineered to output a spectrally pure state with a circularly symmetric JSI, as shown in Figure 1. Figure 1 plots measured data corresponding to 96% spectral purity, obtained using a pump bandwidth of 0.6 nm and average pump power (measured before the fiber incoupling to the SPDC setup) of 87 mW. These data indicate that the SPDC sources produce spectrally pure biphoton states, exceeding our 90% purity target, and should enable high-quality quantum interference.

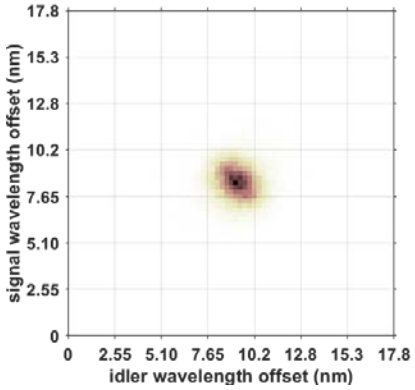

Figure 1. Joint spectral intensity for biphoton state produced by spectrally pure SPDC source. Axis units represent the offset from a reference wavelength; the absolute wavelength value is less important than the scales of the two axes.

The quantum interference visibility, measured in a heralded Hong-Ou-Mandel (HOM) interference experiment, provides another, more important indicator of spectral purity. High-visibility HOM interference is required for multi-span quantum networking operations, including entanglement swapping; thus, the HOM interference visibility provides the most significant and direct metric of spectral purity. The heralded HOM interference setup is illustrated in the left side of Figure 2. The "signal" photons from each source are interfered on a 50-50 beamsplitter, while the "idler" photons from each source are used to herald the presence of their respective signal photons. The right side of Figure 2 plots the detected fourfold coincidence rate as a function of the length difference of the paths traveled by the two signal photons. At zero path length difference, a reduction in fourfold coincidences is observed due to the effect of HOM interference at the 50-50 beamsplitter. A HOM visibility greater than 50% indicates that the interference was quantum mechanical in nature. We have obtained two-source HOM interference with a visibility of (91 ± 3) %, conclusively demonstrating that our SPDC sources produce photons with the qualities required for high-visibility quantum interference.

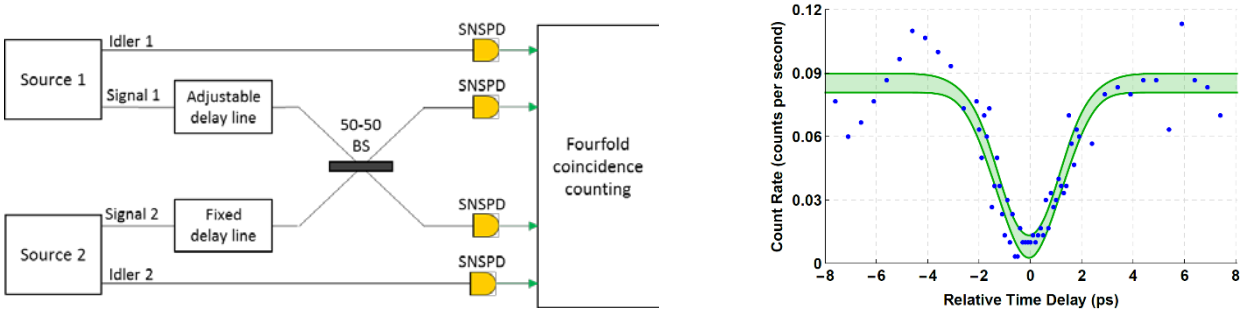

Figure 2. Left: Heralded HOM interference setup. Right: HOM interference between the "signal" photons produced by independent SPDC sources. The green band indicates the 95% confidence interval of the Gaussian fit.

Characterizing the spectral purity achieves one of the requirements for entanglement swapping; the other requirement is analyzing the polarization entanglement. To produce polarization-entangled photon pairs using SPDC, we interfered the outputs of multiple SPDC processes to obtain signal and idler modes entangled in the commonly used Bell state $|\varphi^+>=\frac{1}{\sqrt{2}}(|HH>+|VV>)$. The interferometer was constructed using the "beam displacer scheme," in which the alignment is more stable than in the next best alternative scheme, the "Sagnac interferometer scheme." The beam displacer setup is illustrated in Figure 3. The two SPDC processes are generated in the same PPKTP crystal, in adjacent paths separated by 1 mm, and the physical proximity of the two optical paths helps to reduce phase drift and maintain stable alignment.

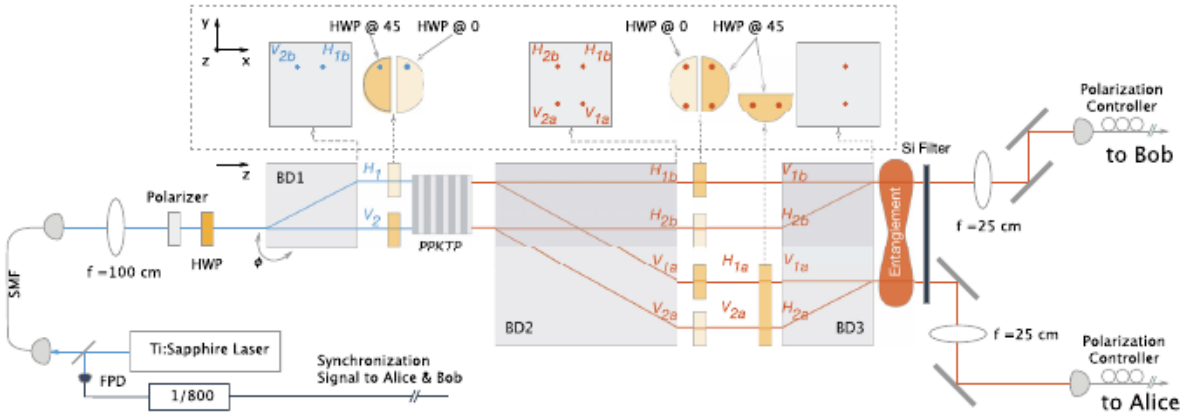

Figure 3. "Beam displacer scheme" for production of polarization-entangled photon pairs. Figure from L. K. Shalm et al, Phys. Rev. Lett. 115 250402 (2015).

The entanglement quality of each individual source was characterized by measuring the visibility of coincidence detections and by measuring the Clauser-Horne-Shimony-Holt (CHSH) *S* parameter, using polarization analyzers comprising a half-wave plate (HWP) plus a polarizing beamsplitter (PBS), as depicted in Figure 4.

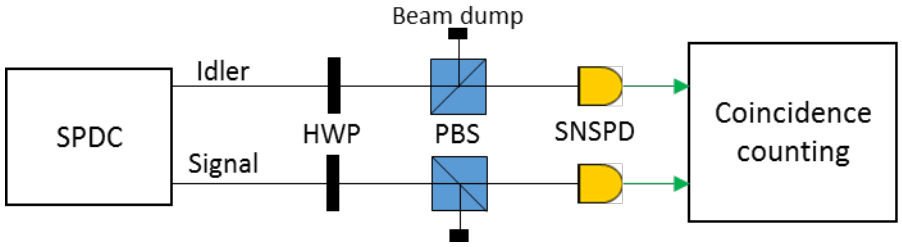

Figure 4. Polarization analysis setup for a single entanglement source.

The coincidence visibility for Source 2 is plotted in Figure 5. To produce this plot, the signal mode's HWP was fixed at four different angles, and for each of those fixed angles, the idler mode's HWP was swept over the range -22.5 – 180 degrees. At each position, the signal-idler coincidences were counted. Signal HWP positions 0 and 45 degrees correspond to the horizontal/vertical (H/V) basis; signal HWP positions 22.5 and 67.5 degrees correspond to the diagonal/antidiagonal (D/A) basis. The coincidence visibilities in each basis, for both sources, are listed in Table 1. A visibility above 71% is considered quantum, and both sources, in both bases, exhibit visibilities above our 90% target.

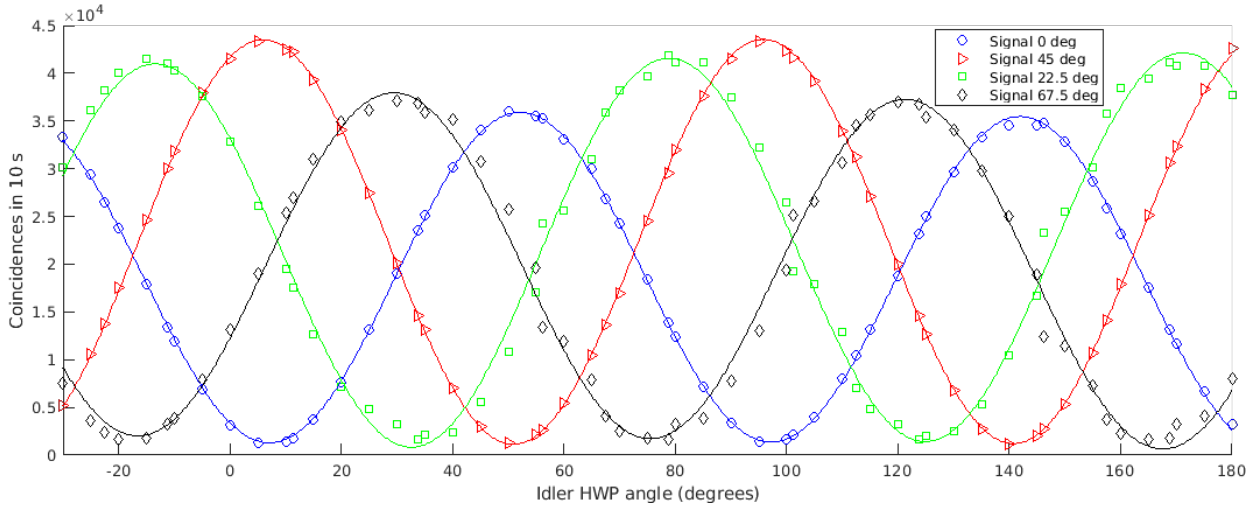

Figure 5. Coincidence visibility, analyzing entanglement of photon pairs produced by Source 2.

Table 1 also lists the values of the CHSH *S* parameter for both sources. The CHSH inequality is one form of a Bell inequality: a value of S > 2 implies that the two modes shared quantum correlations, i.e., were entangled. Both sources produced an *S*-value above the classical bound by 30 standard deviations. The uncertainty was computed by propagating the errors due to Poissonian counting statistics.

TABLE 1

Single-Source Entanglement Characteristics

	H/V basis visibility	D/A basis visibility	CHSH *S*
Source 1	95 %	92 %	2.60 ± 0.02
Source 2	93 %	95 %	2.38 ± 0.01

So far, we have demonstrated high quantum interference visibility (indicating high spectral purity) and produced high-quality polarization-entangled states. The next steps toward multi-span quantum networking are

1. Locally swapping entanglement between the two sources by performing a Bell state measurement on the two signal modes while analyzing the polarization state of the idler modes, and
2. Synchronizing remote entanglement sources to ensure coincident photon arrivals at the Bell state measurement device.

2. SYNCHRONIZING REMOTE ENTANGLEMENT SOURCES ACROSS LINCOLN LABORATORY-MIT FIBER TESTBED

The FY18 synchronization effort has two independent components, the first of which is synchronizing remote SPDC-based entanglement sources, with one source located at Lincoln Laboratory and the other located on MIT campus. The sources need to be synchronized to ensure that the photons produced by both sources temporally overlap at the Bell state measurement device, even when one photon has traveled on a noisy channel like the fiber testbed. This effort involves deriving an 80 MHz master clock signal from the mode-locked pump laser at MIT, transmitting it over the deployed fiber testbed, and using the received signal to drive the mode-locked pump laser at Lincoln Laboratory.

The 80 MHz RF master clock signal is converted to an optical signal at MIT. At Lincoln Laboratory, the received optical signal is converted back to electrical and split. Part of the split signal is used to drive the mode-locked laser, and the other part is used as a reference. The mode-locked laser pulses are detected using a photodiode and compared with the reference signal using a time interval analyzer. The preliminary time interval analyzer tests show 60 ps excess timing jitter between the detected and reference pulses, but we should be able to reduce the measured jitter by improving the test setup. The next step in remote source synchronization involves producing SPDC photons at MIT, multiplexing them with the clock signal, and sending them to Lincoln Laboratory, where they will be detected in a HOM interference setup along with SPDC photons produced at the Laboratory.

3. TOWARD DISTRIBUTED ATOMIC CLOCK NETWORK ACROSS LINCOLN LABORATORY-MIT FIBER TESTBED

The second component of the synchronization effort is transferring/comparing atomic clock signals between Lincoln Laboratory and the Chuang lab at MIT. This component provides greater functionality than does the previous component; besides synchronizing repetition rates, this system will also allow for sharing the phase between two clocks. The current progress is shown in Figure 6.

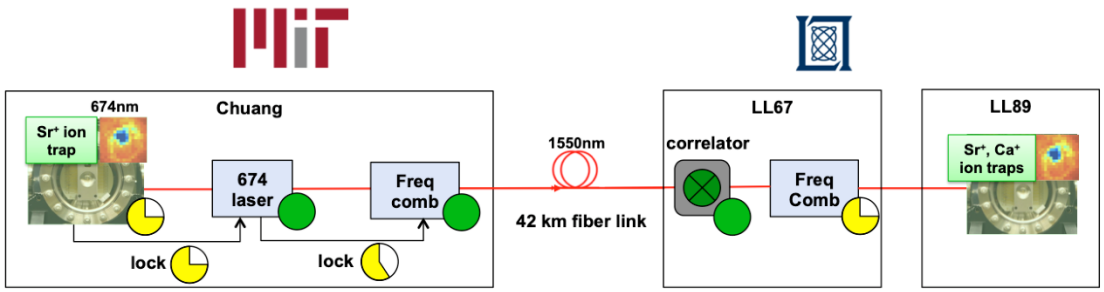

Figure 6. Setup for connecting and comparing remote atomic clocks across Lincoln Laboratory-MIT fiber testbed.

Overall, we have set up each of the pieces required for the experiment, and are working on optimizations to reduce noise levels below thresholds for successful clock transfer and comparison across the Lincoln Laboratory-MIT fiber testbed. Each component is discussed in more detail below:

- Strontium ion clock

  All lasers necessary for cooling and interrogating the ion are now working and stable. We have good ion lifetime in the trap and good Doppler and clock transition spectroscopy. The current coherence time is not yet enough for producing a Ramsey lock signal—we anticipate that optimizing the trapping potentials will further reduce micromotion and improve coherence times to levels suitable for clock spectroscopy.

- 674 laser and ion-674 laser lock

  The 674 laser is now well-stabilized to the ultra-narrow linewidth ULE cavity. The hardware and software are already in place to feed the Ramsey lock signal forward into an acoustic optical modulator (AOM) to keep the laser tracked to the ion transition.

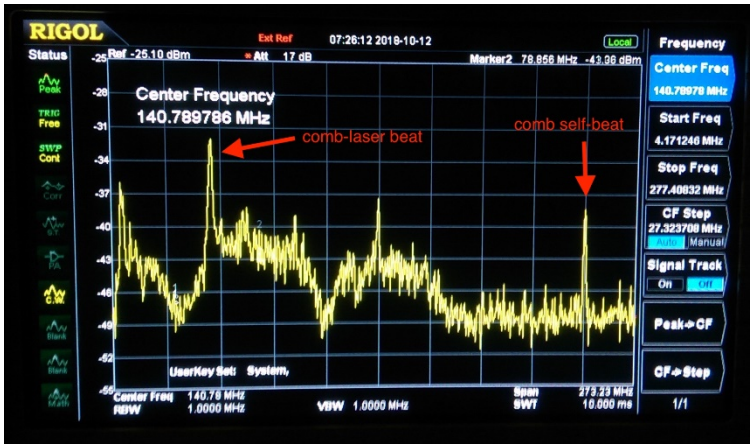

Figure 7. Beat between the frequency comb and the 674 nm laser that is used to interrogate the trapped ion at MIT campus.

- Campus frequency comb and 674-comb stabilization

  The frequency comb is functioning properly and can lock to a commercial clock source. The beat between the comb and 674 laser is shown in Figure 7. We have mixed it down to baseband to generate the lock signal, and are working to improve the SNR so it can be fed into the comb.

- Comb-comb remote comparison

  The cross-correlator has been set up and tested with the Lincoln Laboratory comb in both arms of the input.

- Lincoln Laboratory comb

  The Octavius comb is difficult to operate and outputs light in the visible spectrum, which requires frequency doubling of the campus comb, significantly reducing the cross-correlation signal, so we are planning on taking data with another comb at 1550 nm.

When all components are optimized and combined, this system will allow for comparing and/or transferring both the repetition rate and the phase of clocks in the quantum network fiber testbed. In particular, this system will connect trapped ions, a potential quantum memory technology, to the quantum network testbed.

4. PACKAGING SILICON PHOTONICS FOR QUANTUM AND CLASSICAL APPLICATIONS

In FY18, we received fabricated chips from a collaboration with Group 89, which had been designed in Fall 2015. These chips included large (14 mode, 16 layer) programmable nanophotonic processors (PNPs), ultra-high fidelity PNPs, and on-chip entanglement sources. Our primary goal was to package and construct a test bed for these chips, which we completed for the ultra-high fidelity PNPs.

These ultra-high fidelity PNPs replace the beamsplitters in a conventional Mach-Zehnder Interferometer (MZI) with sub-MZIs of their own. The limiting factor in a conventional MZI is the fact that, due to fabrication imperfections, the beamsplitters are not exactly 50/50. However, by replacing each of these beamsplitters with an MZI, we can tune these devices in-situ, achieving performance limited only by our control and measurement electronics.

Packaging these chips was a technical challenge, requiring collaboration with Group 89 for die dicing and fabrication of electrical fanouts, as well as use of the TOIL lab for manufacturing precision mounts for the chips, ensuring quality mechanical vibration isolation and thermal control. Additionally, custom PCBs, control electronics, and fiber arrays for efficient optical coupling were designed and sourced. The packaged high-fidelity PNP system is pictured in Figure 8. We expect the techniques developed while packaging these chips to be applicable to packaging both the large PNP systems and the integrated entanglement sources.

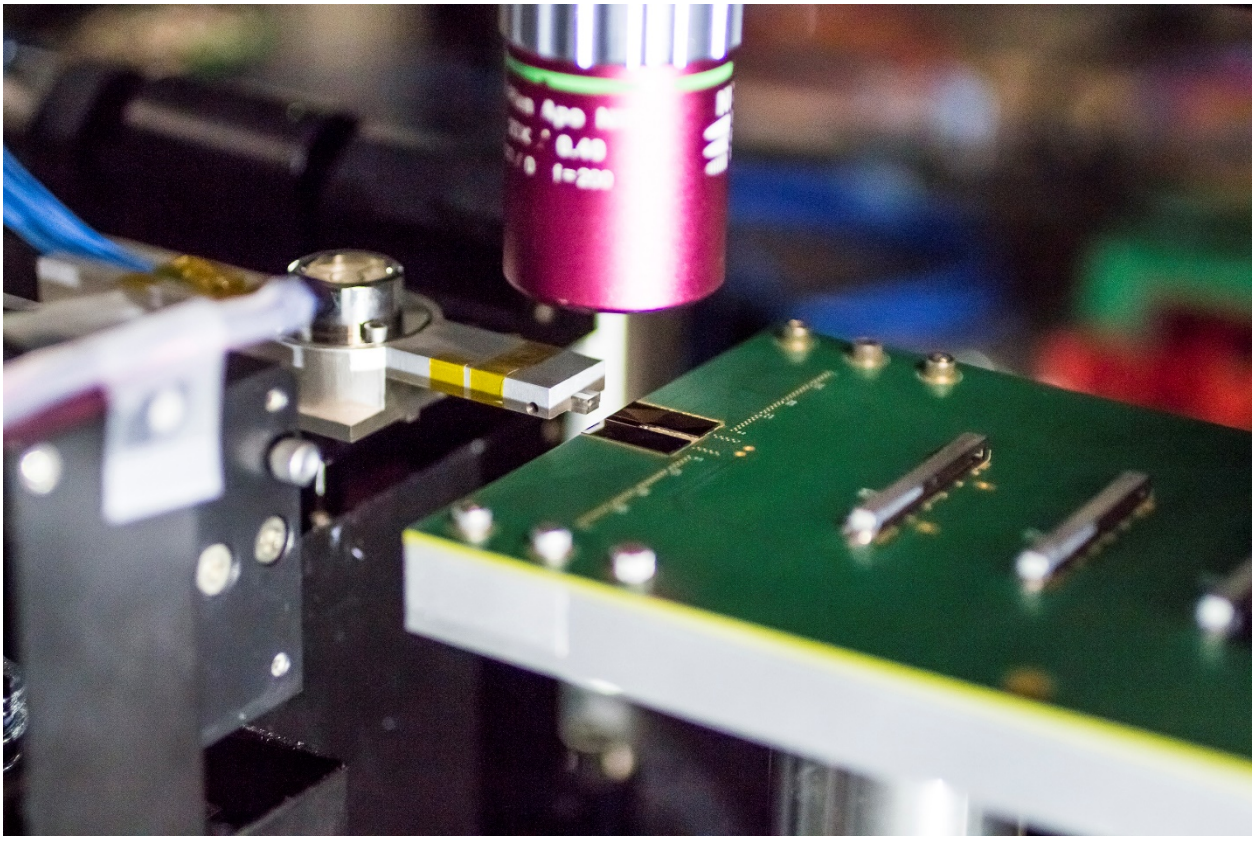

Figure 8. Packaged high-fidelity PNP system, wire-bonded to custom electrical fanouts and then again to a custom PCB. In the background can be seen the custom fiber array that was sourced for optical coupling. The IR objective allows for the monitoring of system operation in-situ.

5. OPTICAL FLOW SWITCHING

FY18 saw a huge amount of progress in the construction and use of a testbed for optical flow switching. Based around an arbitrarily reconfigurable silicon photonics PNP and eight FPGAs running custom IP, we were able to demonstrate optical flow switching for both single- and multi-cast traffic patterns, realizing both latency and throughput improvements in our test network. Figure 9 is a system diagram of the test network, and Figure 10 is a photo of the test network's FPGA bank. Figure 11 shows some test results.

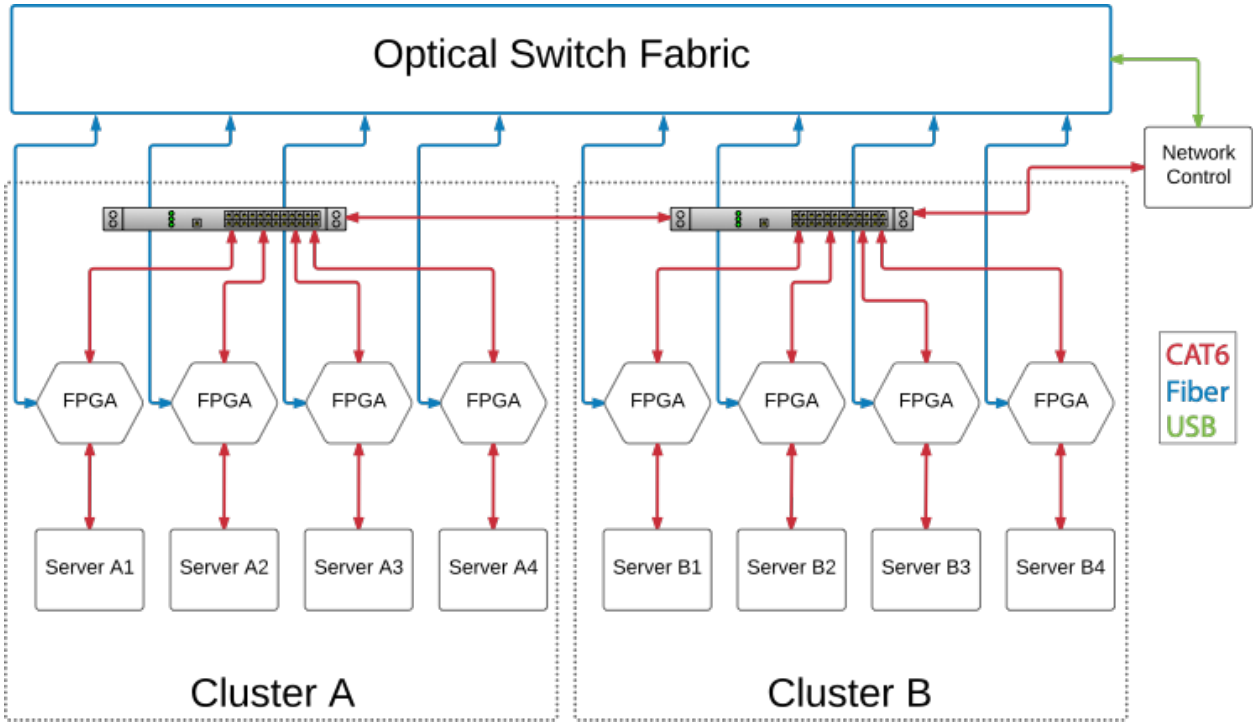

Figure 9. System diagram of optical network testbed. The optical switch fabric is a novel integrated photonics platform, known as a Programmable Nanophotonic Processor, capable of arbitrary linear transformations. This enables both single-cast and multi-cast optical connections

The results of this testing were presented at CLEO 2018 in the paper: "Steinbrecher, Gregory R., et al. "Hybrid Flow Switched Network with an Arbitrarily Reconfigurable Optical Switch." *CLEO: Science and Innovations*. Optical Society of America, 2018."

We have also submitted a patent application for this system: "APPARATUS, SYSTEMS, AND METHODS FOR NONBLOCKING OPTICAL SWITCHING", reference MIT 19503, filed on May 17, 2018.

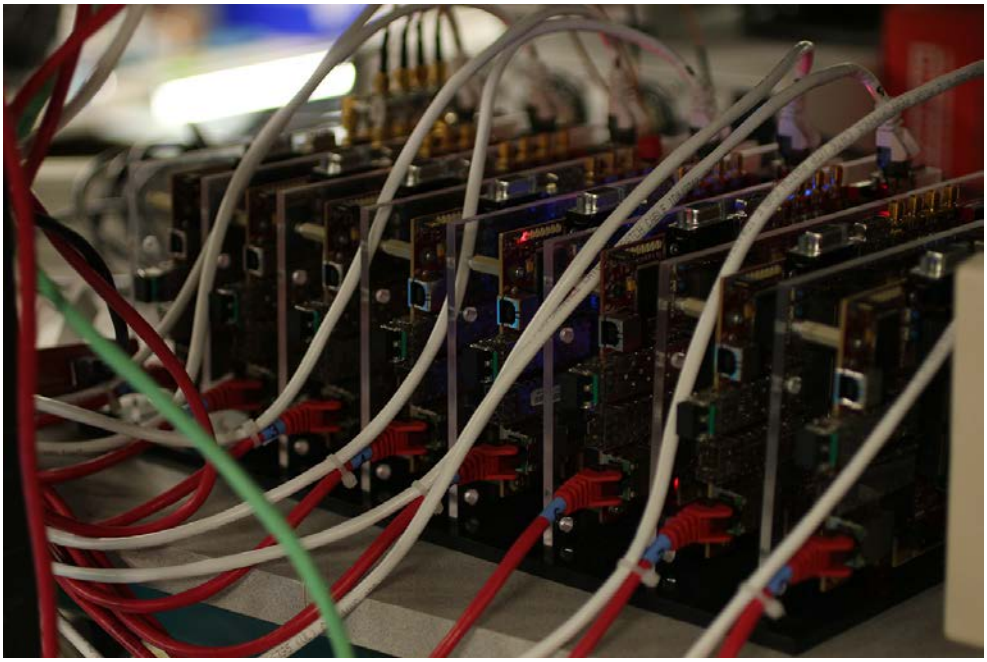

Figure 10. FPGA bank to coordinate traffic mapping to either the optical or electronic layers on a packet-by-packet basis.

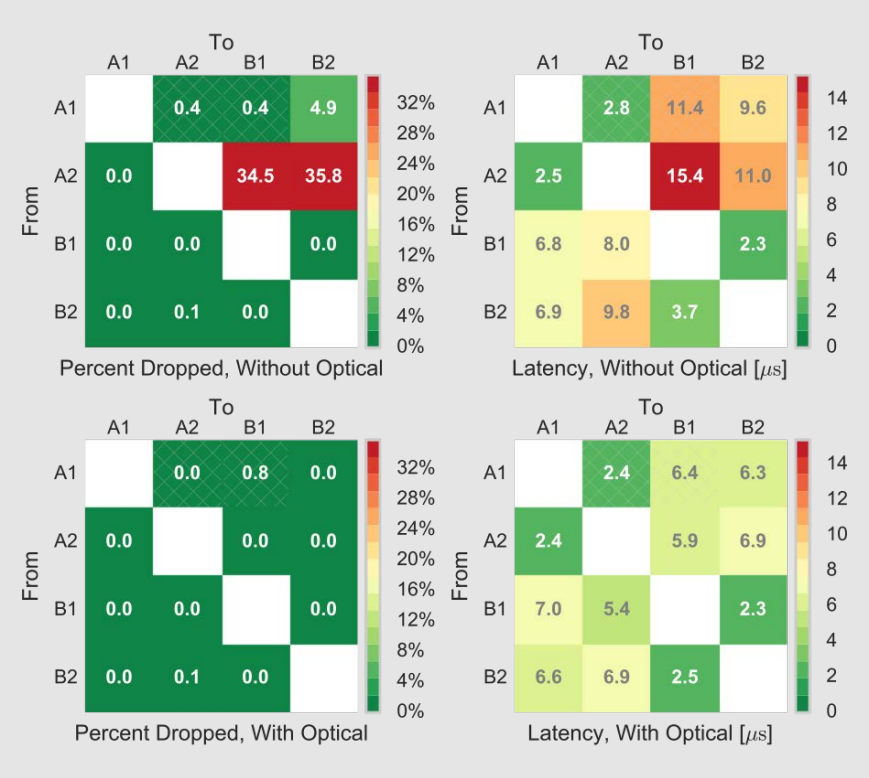

Figure 11. Test results demonstrating latency and packet loss reduction with introduction of optical switching layer. Traffic was 25Mbit all-to-all as well as 300MBit flows from A1->B1 and A1->A2. These elephant flows were switched over the optical layer in the bottom two plots.

In summary, the FY18 integrated photonics effort has produced a packaged device suitable for high-fidelity on-chip entanglement swapping, new techniques applicable for packaging on-chip entanglement sources and large PNPs, and the successful demonstration of optical flow switching to improve classical network performance using a device originally intended for quantum information processing.